PERGAMON

Solid-State Electronics 46 (2002) 1325–1331

SOLID-STATE ELECTRONICS

www.elsevier.com/locate/sse

# A simple approach to understanding measurement errors in the cross-bridge Kelvin resistor and a new pattern for measurements of specific contact resistivity

Mizuki Ono [a,*], Akira Nishiyama [a], Akira Toriumi [b]

[a] *Advanced LSI Technology Laboratory, Corporate Research & Development Center, Toshiba Corporation, 8, Shinsugita-cho, Isogo-ku, Yokohama 235-8522, Japan*

[b] *Department of Material Science, School of Engineering, The University of Tokyo, 7-3-1, Hongo, Bunkyo-ku, Tokyo 113-8656, Japan*

Received 3 September 2001; received in revised form 1 January 2002; accepted 22 January 2002

**Abstract**

Conventionally, the cross-bridge Kelvin resistor (CKR) is used for measurements of specific contact resistivity between metal and silicon. However, this method involves unavoidable measurement errors. They are induced by alignment margins of silicon active layers around contact holes. For the purpose of discussing their physical meanings, a transmission line model approximation and physical considerations are employed. Using the results of these considerations, a new method to avoid measurement errors is proposed. The results measured by using the conventional CKR method and the new method are compared. It is shown that the new method gives physically reasonable results. © 2002 Elsevier Science Ltd. All rights reserved.

*Keywords:* Contact resistance; Specific contact resistivity; Cross-bridge Kelvin resistor; Measurement errors; Alignment margins; Transmission line model

## 1. Introduction

Recently, the miniaturization of transistors has been investigated intensively in many laboratories in accordance with the demands for higher speed operation and lower power consumption [1–7]. Therefore, not only high current drivability but also low parasitic resistance is indispensable. It is expected that specific contact resistivity of a few times $10^{-8}$ $\Omega\,cm^2$ or below will be required for transistors of the sub-50 nm generation [8].

In order to realize extremely low contact resistance, it is important not only to conduct investigations with a view to achieving technical breakthroughs but also to measure contact resistance as accurately as possible. Usually, the cross-bridge Kelvin resistor (CKR) has been used to measure contact resistance. However, it has been pointed out that large measurement errors are unavoidable if CKR is used [9–14]. In order to measure contact resistance more accurately, we propose a new measurement method based on a consideration of the physical meanings of the measurement errors in the CKR method.

## 2. Measurement errors in the cross-bridge Kelvin resistor method

It has been pointed out that measurement errors in the CKR method are induced by alignment margins between active areas and contact holes [9–14]. Some experimental results are shown in Fig. 1. These are for contacts on $n^+$ regions. The contacts were fabricated as follows. After isolation and well fabrication process, As was implanted with a dosage of $2 \times 10^{15}$ $cm^{-2}$ at 50 keV. Then, implanted As was activated with a rapid thermal

* Corresponding author. Tel.: +81-45-770-3693; fax: +81-45-770-3578.

*E-mail address:* m-ono@amc.toshiba.co.jp (M. Ono).

0038-1101/02/$ - see front matter 
PII: S0038-1101(02)00063-1

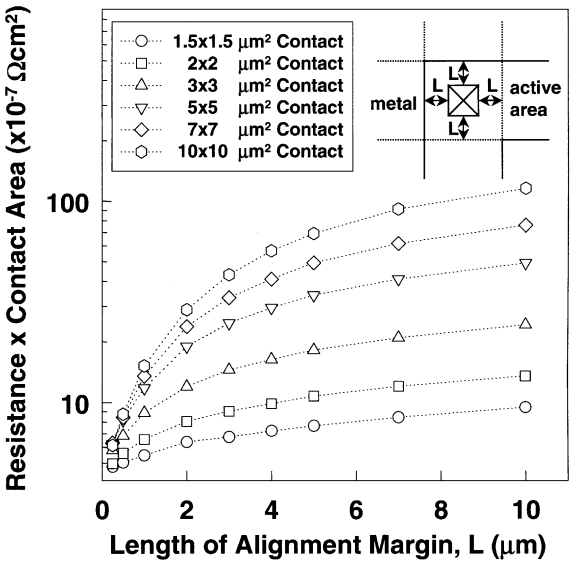


Fig. 1. Dependencies of contact resistance times contact area on alignment margin for As implanted Al–Si–Cu/TiN/Ti/$n^+$ Si.

annealing process at 1000 °C for 30 s. Following the activation process, 800-nm-thick $SiO_2$ was deposited on a wafer and contact holes were opened with a reactive ion etching technique. Next, Al–Si–Cu alloy was sputtered with Ti and TiN as barrier metal underneath it. Then, metal patterning and sintering process were carried out. The area around contact hole is schematically shown in the inset of the figure. Four arrows show alignment margins. All margins are equal. The figure shows dependencies of the product of measured contact resistance by contact area on length of alignment margin. From now on we call this product PMRA (Product of Measured contact Resistance by contact Area). This product agrees with specific contact resistivity in the case that there is no measurement error. It is shown in the next section that CKR without alignment margins gives exact values. Hence, it is known from this figure that the exact specific contact resistivity is about 4 or $5 \times 10^{-7}$ $\Omega\,cm^2$. Therefore, it is seen that measurement error may be an order of magnitude in extreme cases.

Further, as shown in the next section, the CKR method gives larger measurement errors in the case that measured specific contact resistivity is low. Therefore, measurement errors in the CKR method are serious for measuring low specific contact resistivity.

## 3. Physical reasons for measurement errors in the cross-bridge Kelvin resistor

We neglect inhomogeneity of electric current and potential perpendicular to electric current, the thickness of diffusion layer, and resistance of metal. With these

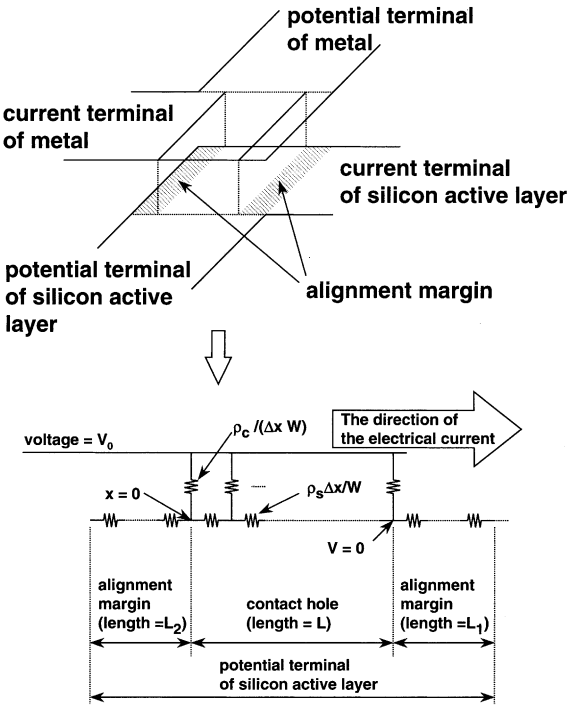


Fig. 2. One-dimensional transmission line model approximation for CKR.

approximations, CKR can be treated with a one-dimensional transmission line model, as shown in Fig. 2. Here, $\rho_c$ is the specific contact resistivity between silicon and metal, $\rho_s$ is the sheet resistance of silicon active layer, $L$ is the length of contact, $L_1$ is the right alignment margin, $L_2$ is the left one, and $W$ is a width of CKR. The origin of coordinate, $x$, is the left edge of contact hole and the origin of potential is that in silicon active layer at the right edge of contact hole. The potential of metal is $V_0$. The measured resistance is the ratio of measured voltage ($V_m$) to electric current ($I$). The measured voltage is the average over potential measurement terminals.

The voltage between metal and silicon active layer, $\Delta V$, is given as

$$\Delta V = \frac{V_0}{\cosh\left(L\sqrt{\frac{\rho_s}{\rho_c}}\right)}, \quad (-L_2 \leqslant x \leqslant 0) \tag{1}$$

$$\Delta V = V_0 \frac{\cosh\left(x\sqrt{\frac{\rho_s}{\rho_c}}\right)}{\cosh\left(L\sqrt{\frac{\rho_s}{\rho_c}}\right)}, \quad (0 \leqslant x \leqslant L) \tag{2}$$

$$\Delta V = V_0\left[1 + \sqrt{\frac{\rho_s}{\rho_c}}\tanh\left(L\sqrt{\frac{\rho_s}{\rho_c}}\right)(x - L)\right], \quad (L \leqslant x \leqslant L + L_1). \tag{3}$$

Hence $V_m$ is given as

$$V_m = \frac{1}{L+L_1+L_2}\int_{-L_2}^{L+L_1}\Delta V\,dx = \frac{V_0}{L+L_1+L_2}\left[\frac{L_2}{\cosh\left(L\sqrt{\frac{\rho_s}{\rho_c}}\right)} + \sqrt{\frac{\rho_c}{\rho_s}}\tanh\left(L\sqrt{\frac{\rho_s}{\rho_c}}\right) + L_1 + \sqrt{\frac{\rho_s}{\rho_c}}\tanh\left(L\sqrt{\frac{\rho_s}{\rho_c}}\right)\frac{L_1^2}{2}\right]. \quad (4)$$

The electric current, $I$, is given as

$$I = \frac{WV_0}{\sqrt{\rho_c\rho_s}}\tanh\left(L\sqrt{\frac{\rho_s}{\rho_c}}\right). \quad (5)$$

Hence, the measured resistance, $R$, is given as

$$R = \frac{\rho_c + \sqrt{\rho_c\rho_s}\coth\left(L\sqrt{\frac{\rho_s}{\rho_c}}\right)L_1 + \frac{\rho_s}{2}L_1^2 + \frac{\sqrt{\rho_c\rho_s}}{\sinh\left(L\sqrt{\frac{\rho_s}{\rho_c}}\right)}L_2}{(L+L_1+L_2)W}. \quad (6)$$

In the case that both $L_1$ and $L_2$ are zero, $R$ is equal to $\rho_c/(LW)$ which is the exact value of contact resistance. However, in the case that either $L_1$ or $L_2$ is not zero, $R$ is not equal to the exact value.

Dependencies of the ratio of calculated PMRA to exact specific contact resistivity on alignment margin are shown in Fig. 3, in the case of $L_1 = L_2$ and $W = 1$ μm. In this calculation, $\rho_c$ and $\rho_s$ were set to $1 \times 10^{-7}$ Ω cm$^2$ and 100 Ω, respectively, and contact length was 1, 2, 5, and 10 μm. This qualitatively agrees with Fig. 1. It is known from this figure that measurement error is larger in the case of longer contact. The reason for this will be given later.

In order to see effects of $L_1$ and $L_2$ on PMRA, measurements were carried out. A schematic view of the pattern is shown in Fig. 4. The fabrication process of these contacts was the same as for those in Fig. 1, except for the implantation dosage of As, which was $5 \times 10^{15}$ cm$^{-2}$. Sizes of contact holes are $2 \times 2$, $5 \times 5$, and $10 \times 10$ μm$^2$. The dependencies of PMRA on $L_1$ are shown in Fig. 5. $L_1$ is varied from 1 to 50 μm, while $L_2$ is fixed to 1 μm. The dependencies of PMRA on $L_2$ in Fig. 4 are shown in Fig. 6. These results qualitatively agree with (6).

These results can be understood qualitatively as follows. It is seen from Eqs. (1)–(3) that voltage between metal and silicon active layer in $L \leqslant x \leqslant L + L_1$ is larger than that in $0 \leqslant x \leqslant L$ and that voltage in $-L_2 \leqslant x \leqslant 0$ is lower than that in $0 \leqslant x \leqslant L$. Therefore, PMRA becomes

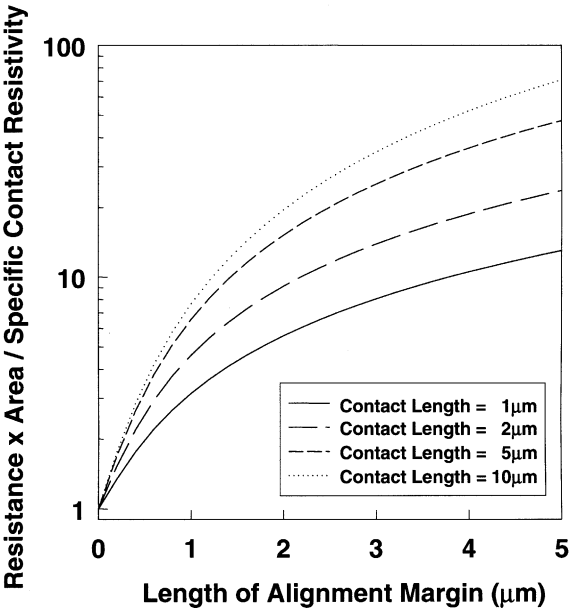


Fig. 3. Dependencies of the ratio of calculated contact resistance times contact area on the alignment margin. In this calculation, exact specific contact resistivity is $1 \times 10^{-7}$ Ω cm$^2$ and sheet resistance of silicon active layer is 100 Ω.

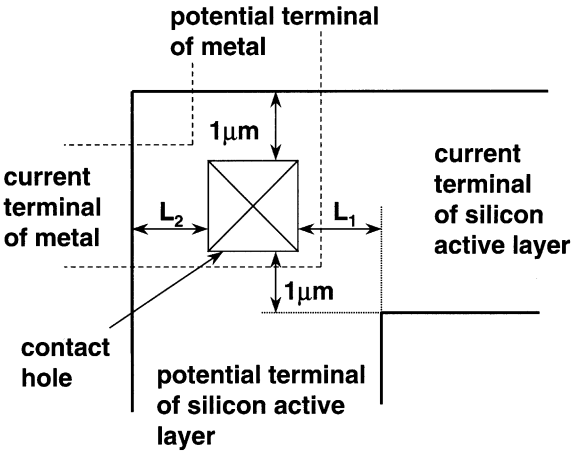


Fig. 4. A schematic view around contact hole.

higher in the case of Fig. 5 and lower in the case of Fig. 6, as alignment margins increase. Further, the dependence of measurement errors on contact length in Fig. 3 is understood qualitatively as follows. First, measured contact resistance is lower in the case that contact length is longer. Second, the measurement error caused by parasitic resistance is larger in the case that measured resistance is lower. Hence, the measurement error is larger in the case that contact length is longer. From the same consideration, it is also known that measurement

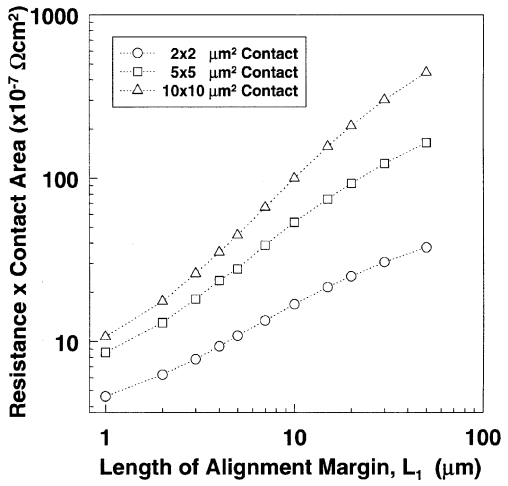


Fig. 5. Dependencies of contact resistance times contact area on $L_1$ in Fig. 4 for As implanted Al–Si–Cu/TiN/Ti/$n^+$ Si. Here, $L_2$ is fixed to 1 μm.

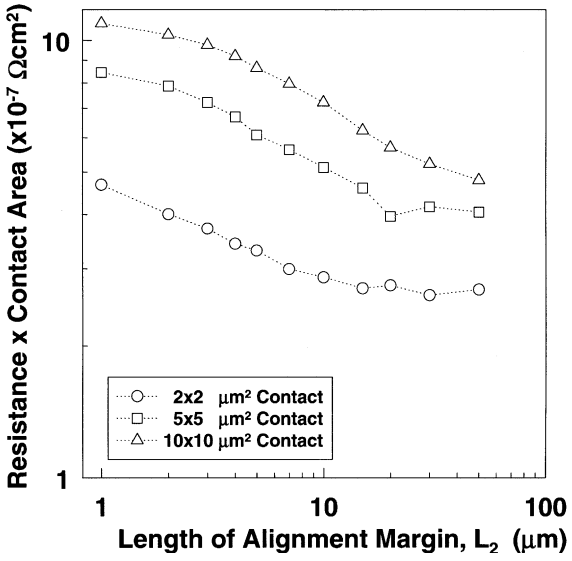


Fig. 6. Dependencies of contact resistance times contact area on $L_2$ in Fig. 4 for As implanted Al–Si–Cu/TiN/Ti/$n^+$ Si. Here, $L_1$ is fixed to 1 μm.

error is larger in the case that specific contact resistivity is lower.

## 4. A new method

It has been shown in the previous sections that large measurement errors in the CKR method are induced by using average values for the measurements. Therefore, not to use average values is important in order to avoid measurement errors. We propose a novel pattern in order to extract the correct specific contact resistivity.

In the extreme case that the length of the contact hole, $L$, is sufficiently longer than $(\rho_c/\rho_s)^{1/2}$, the value of current given by (5) can be described as

$$I = \frac{WV_0}{\sqrt{\rho_c \rho_s}}. \tag{7}$$

Because of Eq. (2), the voltage at the right edge of contact hole in Fig. 2 is $V_0$. Hence, if the ratio of voltage at the edge of contact hole to electric current and $\rho_s$ are known, $\rho_c$ is obtained by dividing the square of the ratio with $\rho_s$. In order to measure the ratio with as small an error as possible, disturbance of the electric current and/or potential near the edge of contact hole must be as small as possible. Hence, there must be no measurement terminal for potential in silicon active layer near the edge of contact hole. Our pattern is schematically shown in Fig. 7. The fundamental idea is the same as that of the Shockley Pattern [15]. Electric current flows between the "current terminal of metal" and the "current terminal of silicon active layer". The ratio of voltage at the edge of contact hole to electric current is obtained by extrapolating the ratio of voltage between the "potential terminal of metal" and each "potential terminal of silicon active layer" to electric current. Different from the Shockley Pattern in [15], potential measurement terminals are placed beside the silicon active layer. Hence, their disturbance of electric current and potential can be diminished by setting the width of silicon active layer sufficiently wide. Further, for the approximation (7) to be correct, the length of contact hole parallel to electric current must be sufficiently long. In our experiment, the width and length of contact hole are 10 and 500 μm,

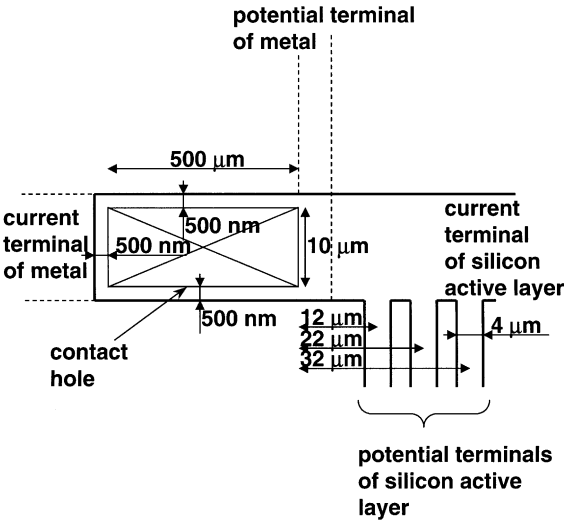


Fig. 7. A schematic view of the new pattern.

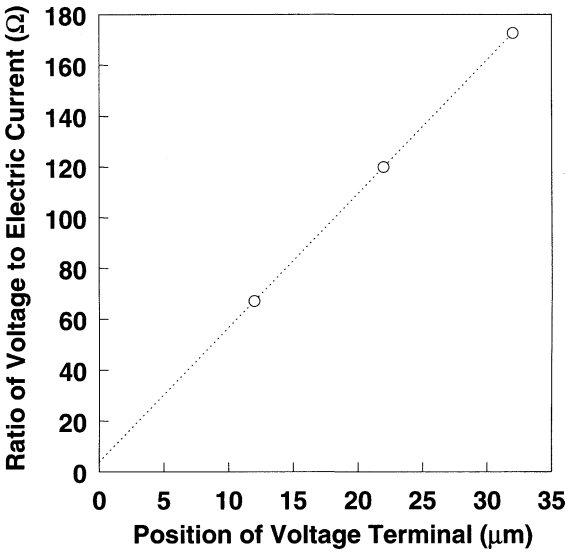


Fig. 8. Dependence of the ratio of voltage to electric current on position of potential measurement terminal for As implanted Al–Si–Cu/TiN/Ti/$n^+$ Si.

respectively. The alignment margins at top, bottom, and left of contact hole in Fig. 7 are all 500 nm. The distances between the edge of contact hole and the center of each "potential terminal of silicon active layer" are 12, 22, and 32 μm. Their widths are 4 μm. An experimental dependence of the ratio on the position of "potential terminal of silicon active layer" is shown in Fig. 8. This is for a contact on an $n^+$ region, in which As was implanted with a dosage of $5 \times 10^{15}$ $cm^{-2}$ at 50 keV. The metal is Al–Si–Cu alloy with Ti and TiN as barrier metal underneath it. Linearity of the graph is good. Hence, both approximations, which are used in our method, and the extrapolation are justified.

Some PMRA are shown in Fig. 9. These are for contacts on $n^+$ regions, in which As was implanted with a dosage of 1, 2, and $5 \times 10^{15}$ $cm^{-2}$ at 50 keV. The metal is Al–Si–Cu alloy with Ti and TiN as barrier metal underneath it. Here, open and filled symbols show results obtained by using CKR and the new pattern, respectively. In the case of measurements with CKR, sizes of contacts are $5 \times 5$ and $10 \times 10$ $\mu m^2$ and all alignment margins, which are shown in the inset in Fig. 1, have equal lengths. For all implantation conditions, large symbols show results of $10 \times 10$ $\mu m^2$ contacts and small symbols show results of $5 \times 5$ $\mu m^2$ contacts. These are averaged values over six chips in each wafer. In the case of some data, error bars are shorter than the size of symbols. Regression lines for results with CKR are also shown with dotted lines. The horizontal axis shows the length of alignment margin of CKR. The sheet resistances of silicon active layers were measured by using the conventional four terminal pattern and the values

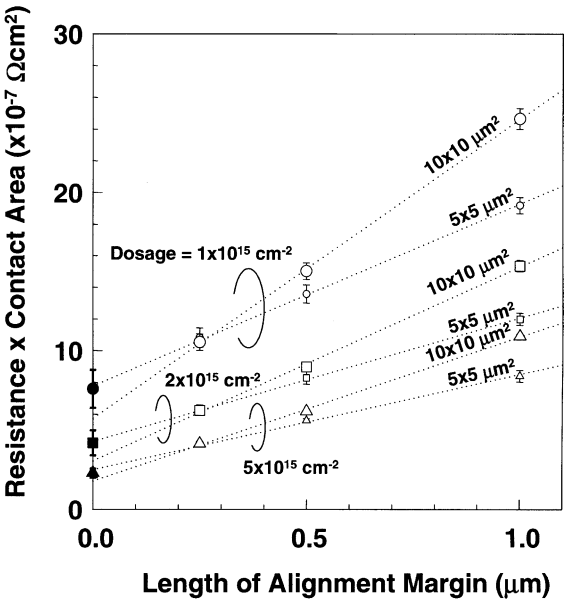


Fig. 9. Dependencies of contact resistance times contact area on length of alignment margin for As implanted Al–Si–Cu/TiN/Ti/$n^+$ Si. Here, open and filled symbols show results obtained by using CKR and the new pattern, respectively.

were 108, 75, and 60 Ω for the cases of As dosage of 1, 2, and $5 \times 10^{15}$ $cm^{-2}$, respectively. Results for contacts on $p^+$ regions, in which B was implanted with a dosage of 1, 2, and $5 \times 10^{15}$ $cm^{-2}$ at 30 keV, are shown in Fig. 10.

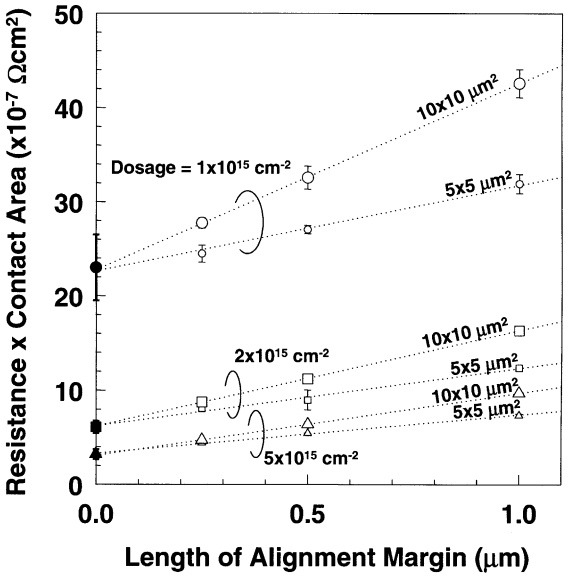


Fig. 10. Dependencies of contact resistance times contact area on length of alignment margin for B implanted Al–Si–Cu/TiN/Ti/$p^+$ Si. Here, open and filled symbols show results obtained by using CKR and the new pattern, respectively.

Also in this figure, results with CKR and new pattern and regression lines for results with CKR are shown and sizes of contacts in CKR are $5 \times 5$ and $10 \times 10$ μm$^2$. The sheet resistances of silicon active layers were 97, 53, and 36 Ω for the cases of B dosage of 1, 2, and $5 \times 10^{15}$ cm$^{-2}$, respectively. In these figures, all filled symbols agree with the extrapolated value of graphs of open symbols to the point where alignment margin is zero. This is physically reasonable.

## 5. Discussions

As shown in the previous section, the values of specific contact resistivity obtained by using the new pattern agree with those obtained by extrapolating the results of the CKR method. In the cases of results for contacts on $p^+$ regions, which are shown in Fig. 10, values obtained with the new pattern agree quite well with those obtained with linear extrapolation of CKR results. However, in the case of results for $10 \times 10$ μm$^2$ contacts on $n^+$ regions, which are indicated by the larger symbols in Fig. 9, values obtained with the new pattern are slightly higher than those obtained by linear extrapolation. The reason for these discrepancies can be understood as follows.

Within one-dimensional approximation, PMRA in Figs. 9 and 10 can be estimated by putting $L_1 = L_2$ in (6). Within this approximation, PMRA increase faster than linear function of alignment margin. To be precise, graphs of PMRA dependencies on alignment margin are not lines but curves. Hence, linear extrapolation of PMRA, which is obtained with conventional CKR, underestimates specific contact resistivities, i.e., exact values of specific contact resistivities are higher than values obtained with linear extrapolation. It is known from Eq. (6) that linear approximation to PMRA dependence on alignment margin becomes worse as lengths of contact holes increase. Hence, the values obtained with extrapolation are expected to be lower in the case of $10 \times 10$ μm$^2$ contacts than in the case of $5 \times 5$ μm$^2$ contacts. It is also known from Eq. (6) that linear approximation to PMRA dependence on alignment margin becomes worse as ratios of sheet resistance to specific contact resistivity increase. In the case of this experiment, the ratios in contacts on $n^+$ regions are larger than those on $p^+$ regions. Hence, the agreement between extrapolation and the new method is expected to be worse in the case of contacts on $n^+$ regions than in the case of those on $p^+$ regions. Therefore, the discrepancy between values with extrapolation and values with the new method is expected to be largest in the case of $10 \times 10$ μm$^2$ contacts on $n^+$ regions. These reasons account for the discrepancies between values obtained with the new pattern and those obtained by linear extrapolation of results for $10 \times 10$ μm$^2$ contacts on $n^+$ regions and for the fact that results with the new pattern agree well with linear extrapolation of CKR in the cases of $5 \times 5$ μm$^2$ contacts on $n^+$ regions and contacts of both sizes on $p^+$ regions.

It should be noted that in the case of measurement of extremely low specific contact resistivities, the ratios of sheet resistance to specific contact resistivity are large. In those cases, it is difficult to estimate specific contact resistivities by extrapolating results with CKR, since linear extrapolation cannot be justified. Hence, it is difficult to use the conventional CKR method for measurements of extremely low specific contact resistivities. On the contrary, in the case of the new method, there is no restriction on the value of specific contact resistivities. Hence, this proposed method is considered to be effective for measurements of low specific contact resistivity without suffering from large measurement errors.

## 6. Summary and conclusion

The conventional CKR for the measurement of specific contact resistivity involves unavoidable measurement errors. The errors are larger in the case that measured contact resistance is low. Hence, the conventional CKR is inappropriate for measurements of low specific contact resistivity. The physical meanings of measurement errors were considered. Using the results of this consideration, we proposed a new method. The values of specific contact resistivity obtained by using this method are physically reasonable. Therefore, this new method is effective for measurements of low specific contact resistivity without suffering from large measurement errors.

## Acknowledgements

The authors would like to thank members of the Advanced LSI Technology Laboratory, Corporate Research and Development Center, Toshiba Corp., for useful discussion and comments, and in particular Dr. K. Matsuzawa for his enlightening comments on numerical simulations during the mask pattern designing. The authors are also grateful to staff at the Microelectronics Center, Toshiba Corp., for the support they extended regarding sample fabrication.

## References

[1] Toriumi A, Mizuno T, Iwase M, Takahashi M, Niiyama H, Fukumoto M, Inaba S, Mori I, Yoshimi M. High speed 0.1 μm CMOS devices operating at room temperature. Ext Abs of the 1992 International Conference on Solid State Devices Materials. p. 487–9.

[2] Hashimoto T, Sudoh Y, Kurino H, Narai A, Yokoyama S, Horiike Y, Koyanagi M. 3 V operation of 70 nm gate length MOSFET with new double punch through stopper structure. Ext Abs of the 1992 International Conference on Solid State Devices Materials. p. 490–2.
[3] Hori A, Nakaoka H, Umimoto H, Yamashita K, Takase M, Shimizu N, Mizuno B, Odanaka S. A 0.05 μm-CMOS with ultra shallow source/drain junctions fabricated by 5 keV ion implantation and rapid thermal annealing. IEDM Tech Dig (December) 1994:485–8.
[4] Ono M, Saito M, Yoshitomi T, Fiegna C, Ohguro T, Iwai H. A 40 nm gate length nMOSFET. IEEE Trans Electron Dev 1995;42(10):1822–30.
[5] Ono M, Saito M, Yoshitomi T, Fiegna C, Ohguro T, Momose HS, Iwai H. Fabrication of sub-50-nm gate length n-metal-oxide–semiconductor field effect transistors and their electrical characteristics. J Vac Sci Technol B 1995; 13(4):1740–3.
[6] Tsuji K, Takeuchi K, Mogami T. High performance 50-nm physical gate length pMOSFETs by using low temperature activation by re-crystallization scheme. Tech Dig of 1999 Symposium on VLSI Technology, p. 9–10.
[7] Chau R, Kavalieros J, Roberds B, Schenker R, Lionberger D, Barlage D, Doyle B, Arghavani R, Murthy A, Dewey G. 30 nm physical gate length CMOS transistors with and 1.0 ps n-MOS 1.7 ps p-MOS gate delays. IEDM Tech Dig (December) 2000:45–8.
[8] International Technology Roadmap for Semiconductors. Available at http://public.itrs.net/.
[9] Loh WM, Saraswat K, Dutton RW. Analysis and scaling of kelvin resistors for extraction of specific contact resistivity. IEEE Electron Dev Lett 1985;EDL-6(3): 105–8.
[10] Schreyer TA, Saraswat KC. A two-dimensional analytical model of the cross-bridge Kelvin resistor. IEEE Electron Dev Lett 1986;EDL-7(12):661–3.
[11] Scorzoni A, Finetti M, Grahn K, Suni I, Cappelletti P. Current crowding and misalignment effects as sources of error in contact resistivity measurements—Part I: Computer simulation of conventional CER and CKR structures. IEEE Trans Electron Dev 1987;ED-34(3):525–31.
[12] Cappelletti P, Finetti M, Scorzoni A, Suni I, Circelli N, Libera GD. Current crowding and misalignment effects as sources of error in contact resistivity measurements—Part II: Experimental results and computer simulation of self-aligned test structures. IEEE Trans Electron Dev 1987;ED-34(3):532–6.
[13] Gillenwater RL, Hafich MJ, Robinson GY. The effect of lateral current spreading on the specific contact resistivity in D-resistor Kelvin devices. IEEE Trans Electron Dev 1987;ED-34(3):537–43.
[14] Santander J, Lozano M, Cané C. Accurate extraction of contact resistivity on Kelvin D-resistor structures using universal curves from simulation. IEEE Trans Electron Dev 1993;40(5):944–50.
[15] Yu AYC. Electron tunneling and contact resistance of metal-silicon contact barriers. Solid-State Electron 1970; 13:239–47, and references therein.